Multifunctional Nanowires and Hierarchical 3D Nanostructures of Material Composites for Energy Storage

IOP Conf. Series: Journal of Physics: Conf. Series **1463** (2020) 012036 doi:10.1088/1742-6596/1463/1/012036

Multifunctional Nanowires and Hierarchical 3D Nanostructures of Material Composites for Energy Storage

B Vidyadharan[1], B Pal[1], I I Misnon[1], H I Elim[2], R Jose[1]*

[1] Nanostructured Renewable Energy Materials Laboratory, Faculty of Industrial Sciences & Technology, Universiti Malaysia Pahang, Malaysia.
[2] Department of Physics, University of Pattimura, Ambon, Indonesia.

* E-mail: rjose@ump.edu.my

Abstract. Composites of functional materials have long been synthesized for achieving enhanced physical and chemical properties. In this era of energy intensive electronics and electric vehicles, energy storage devices utilising composite materials could offer improved performance at a lower cost. Furthermore, if the composite materials are synthesized in one-dimensional morphology at a nano level, conductivity and thus electrical properties could be multiplied. A range of materials with different functionalities have been synthesized by our group recently; as a typical example synthesis of a composite nanowire containing NiO and CuO for supercapacitive energy storage is detailed in this paper and compared the performance of the composite wires with its component binary wires. The materials were synthesized by electrospinning technique and characterized for their structure, microstructure, surface properties and electrochemical properties. The results shows that a composite wire containing materials for similar electrical conductivity would lead to improved charge storage performance than their single component counterparts.

1. Introduction

A fast growing market for portable electronic devices and hybrid electric vehicles (HEVs) and hybrid electric vehicles has led to intense research in the area of electrical energy storage devices characterized by high energy densities (≈ 100-200 $WhKg^{-1}$), power densities (≥5 $kWkg^{-1}$) and a long cycle life (≥10^5 cycles) [1,2]. Supercapacitors are a class of energy storage devices including electric double layer capacitors, pseudocapacitors, and hybrid capacitors [3,4]. Electric double layer capacitors (EDLCs) store electrical energy via the accumulation of electric charges at an electrical double layer formed at the interface between a mesoporous electrode and electrolyte. Carbon structures such as activated carbon, carbon nanotubes, and graphene have been chosen to build EDLCs. No electron transfer takes place across the electrode-electrolyte interface. Transition metal oxides (TMOs) and conducting polymers show high pseudo-capacitance equal to F/ (ΔE × m), where F is the faraday constant, m is the molecular weight and ΔE is the redox potential of the material. High electrical conductivity (conductivity of RuO_2), large surface area (>10 cm^2/g), ability to undergo reversible faradaic electrochemical reactions, an array of oxidation states in the electrode materials to accommodate electrons of varying energy, and faster ion diffusivity are properties of TMOs and electrolytes required to achieve higher energy and power densities in pseudocapacitors [5,6]. The hybrid capacitors combine the properties of EDLC and pseudocapacitors.

The 1D morphologies offer a cylindrical distribution of charges and directed charge transport; therefore, they have high electrical conductivities [7]. Moreover, increased surface area of low diameter nanowires helps in maximum utilisation of active electrode materials [8]. Various chemical methods are utilised to synthesize 1D morphologies of supercapacitor electrode material. However, compared with other processes adopted, electrospinning is a simple, versatile and cost-effective method to produce low diameter 1D nanostructures [7,9–11]. In the electrospinning technique, a polymeric solution, usually prepared in an organic solvent, is injected through a syringe needle in the presence of an electric field. A polymeric jet is initiated upon injection of the solution that undergoes asymmetric bending during the passage between the injector and the collector. This asymmetric bending increases the path length of the jet and allows the solvent to evaporate thereby producing solid continuous fibres with diameters ranging from nanometres to sub-micrometres on a collector surface. If the polymeric solution contains precursors for forming an inorganic solid, then appropriate annealing produces its continuous nanofibres [12,13].

In the recent past, our group has synthesized an array of composite materials as nanowires and 3D nanostructures for their application in catalysis [14,15], solar cells [14,16–19], and charge storing electrodes [20–25]. In most of the previous works, a highly conducting and a highly capacitive with large surface area has been reported. However, a composite with similar electrical conductivity and surface properties were not considered before. This paper addresses this gap and describes the synthesis and characterization of a composite wire containing two ceramics, viz. NiO and CuO and evaluation of their suitability as a supercapacitive charge storing electrode.

2. Experimental Details

The CuO – NiO hybrids as well as their individual components were synthesized by electrospinning technique as reported before [26,27]. For synthesis of CuO – NiO hybrids, the metal precursors were in 1:1 molar ratio (no other ratios made a composite). Starting materials used were; cobalt acetate tetrahydrate [$Cu(CH_3COO)_2$. $4H_2O$; CuAc; 99%; Sigma Aldrich, USA], nickel acetate tetrahydrate [$Ni(CH_3COO)_2.4H_2O$; NiAc; 99%; Sigma Aldrich, USA] and polyvinyl alcohol (PVA; Mw-145,000, Merck). For preparing hybrid, the precursors of cobalt and nickel was taken in a 1:1 molar ratio and dissolved in 7 wt% of PVA solution. With slow and continuous stirring for 24h, a clear solution was obtained. This clear solution was electrospun using a commercial electrospinning unit (Electroris, nanoLab, Malaysia) at 0.6 mL h^{-1} and at ~18 kV. The as-spun fibres are collected on an aluminium foil at a distance ~ 15 cm from the spinneret. The relative humidity around spinning unit was maintained at ~ 30%. The resultant product was calcined at 450 ^oC for 1 h in air to remove the polymer and complete nucleation of nanocomposite.

The crystal structure of each materials were studied by X-ray diffraction (XRD) using a Rigaku Miniflex II X-ray diffractometer employing Cu Kα radiation (λ = 1.5406 °A). The morphology and microstructure of the materials were studied by scanning electron microscopy (7800F, FESEM, JEOL, USA). High resolution lattice images and selected area diffraction patterns were obtained using transmission electron microscopy (TEM) operating at 300 kV (FEI, Titan 80–300 kV). X-ray photoelectron spectroscopy (XPS) was employed to verify the elemental composition of the composite.

The electrochemical properties of material and asymmetric supercapacitor (ASC) were measured using potentiostat-galvanostat (PGSTAT M101, Metrohm Autolab B.V., Netherlands) employing NOVA 1.9 software. Cyclic voltammetry (CV), charge-discharge cycles (CDC), electrochemical impedance spectroscopy (EIS) measurements were carried out using potentiostat at room temperature. A platinum rod and a saturated Ag/AgCl electrode were used as the counter and the reference electrodes, respectively. Electrolyte used was 6M KOH because of its high ionic conductivity (626.6 $mScm^{-1}$). A normalized mass-loading range from ~2.0-2.5 $mgcm^{-2}$ of the active material was used for

the experiments. The ASCs were fabricated by assembling the NiO – CuO composite electrodes and the AC electrodes as anode and cathode separated by a glass microfiber filter (fioroni) in 6 M KOH.

3. RESULTS AND DISCUSSION

Fig. 1 compares the XRD pattern of the NiO+CuO composite wire with those of their single component counterparts. Diffraction peaks are seen distinctly at the respective angles for both CuO and NiO. All the CuO peaks fit well to a monoclinic unit cell (Space group $C12/c_1$, #15) with lattice parameters a = 4.598 Å, b = 3.46 Å, c= 5.135 Å and β = 99.30°,[26, 28] which correspond to reported values (PDF Card No: 45-0937) and all the NiO peaks fit well to a cubic structure phase group $Fm\bar{3}m$ with lattice constant a = 4.18 Å[28].

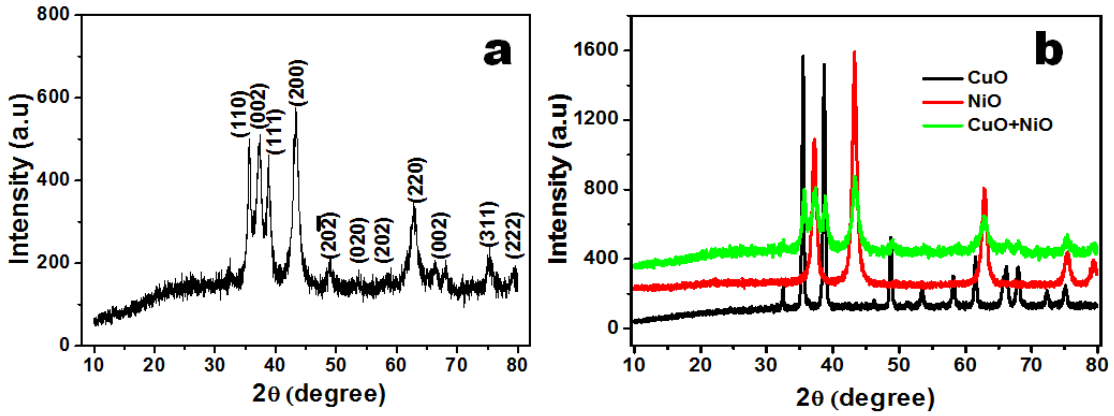

Figure 1. XRD pattern of (a) NiO+CuO composite nanowire (b) composite and its components.

Fig. 2(a) shows SAED pattern corresponding to HRTEM image consists of diffraction spots oriented in a typical polycrystalline ring pattern which further confirm the high degree of particle orientation in the nanowire and those diffraction rings are indexed to (11-3) with d spacing 0.1511 nm, (111) with d spacing 0.2301 nm and (002) with d spacing 0.2519 nm which is consistent with the XRD of CuO. The HRTEM image depicted in Fig. 2(b) reveals the lattice spacing of 0.18 nm, the distance between two (202) planes, indicating the presence of CuO. The lattice spacing 0.25 nm, corresponding the distance between two (002) planes showing the presence of CuO.

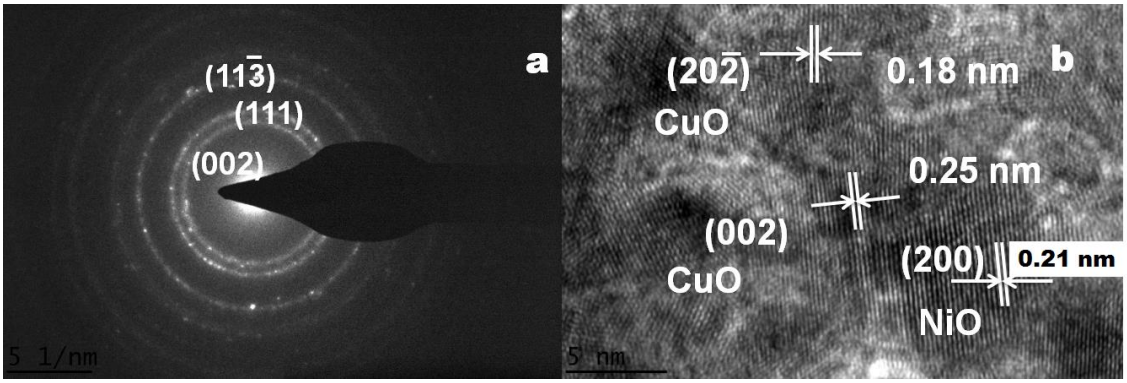

Figure 2. TEM images of CuO+NiO nanowires (a) selected area electron diffraction image, (b) high resolution lattice image of a typical particle in the TEM image.

Fig. 3 shows the FESEM images of the calcined NiO+CuO composite nanowires having uniform diameter ranging from 90 -120 nm. Lower diameter of the wires was further confirmed by TEM measurements (Fig. 3c and d).

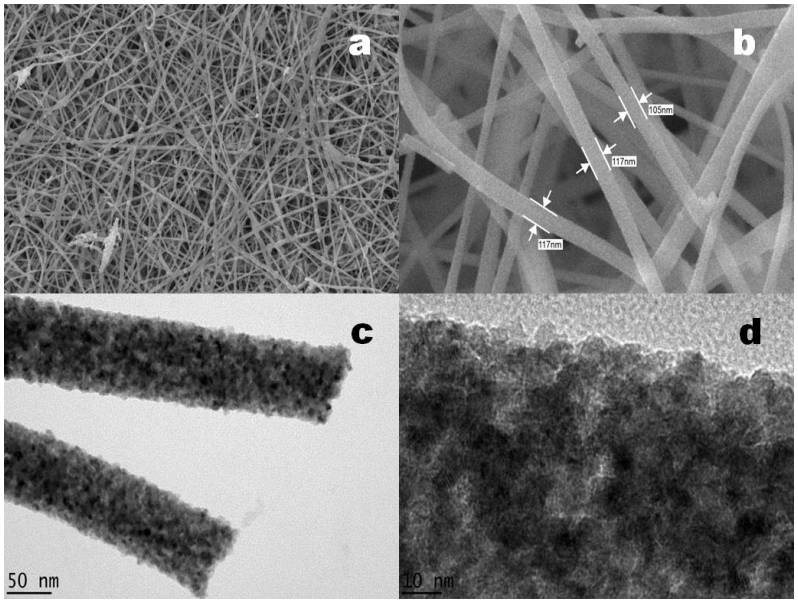

Figure 3. (a-b) FESEM images and (c&d) Bright field TEM images of NiO+CuO nanowires with different magnification.

One of the main criteria for a supercapacitor electrode material is its surface structure. The surface properties of the ceramic nanowires used in this work were studied by gas adsorption technique. Table 1 shows the results obtained from the BET analysis of CuO nanowire, NiO nanowire, and CuO+NiO composite nanowire. The surface area, pore volume and pore size nearly same for all materials due to the similarity of the synthetic procedure. The measured BET surface area of the nanowires was ~14 m^2g^{-1} with a pore volume ~0.5 cm^3g^{-1}, which are at lower end for wires of diameter ~30 – 50 nm. The observed relatively lower surface area is partly contributed by dense particle packing in the wires that reduced porosity despite the lower wire diameter. The Barrett-Joyner-Halenda (BJH) analysis showed a mean pore size of ~11.2 – 11.6 nm because the dense particle packing resulted in larger pores.

Table 1. The specific surface area, total pore volume and mean pore size of all materials.

Materials	**Surface area (m^2g^{-1})**	**Pore volume (cm^3g^{-1})**	**Mean pore size (nm)**
CuO	14.5	0.5	11.5
NiO	13.7	0.5	10.6
NiO+CuO	14.1	0.5	11.6

Fig. 4 shows the CV of NiO+CuO composite nanowire electrode in the potential window -0.2 – 0.5 V. The peak current of the NiO+CuO composite are much higher than single components, indicating that the composite nanowire shows higher electrochemical performance. There are two oxidation peaks (A_1&A_2) observed in the anodic scan and one broad reduction peak C in the cathodic scan. From cathodic peak potentials of CuO (C_1&C_2) and NiO (C_1&C_2) it justified that the cathodic peak C of NiO+CuO composite (Fig. 4(d)) is the integrated cathodic peaks of CuO and NiO. The anodic peaks of

NiO+CuO composite correspond to anodic peaks of CuO (A_1&A_2) and anodic peak of NiO (A). Therefore, all of the peaks from both CuO and NiO are present in the CV of NiO+CuO composite nanowire and the electrochemical redox reaction is ascribed to the following processes [26,27].

$$2CuO + H_2O + 2e^- \underset{Discharging}{\overset{Charging}{\rightleftharpoons}} Cu_2O + 2OH^-$$

$$Cu(OH)_2 + e^- \underset{Discharging}{\overset{Charging}{\rightleftharpoons}} CuOH + OH^-$$

$$NiO + OH^- \leftrightarrow NiOOH + NiO + e^-$$

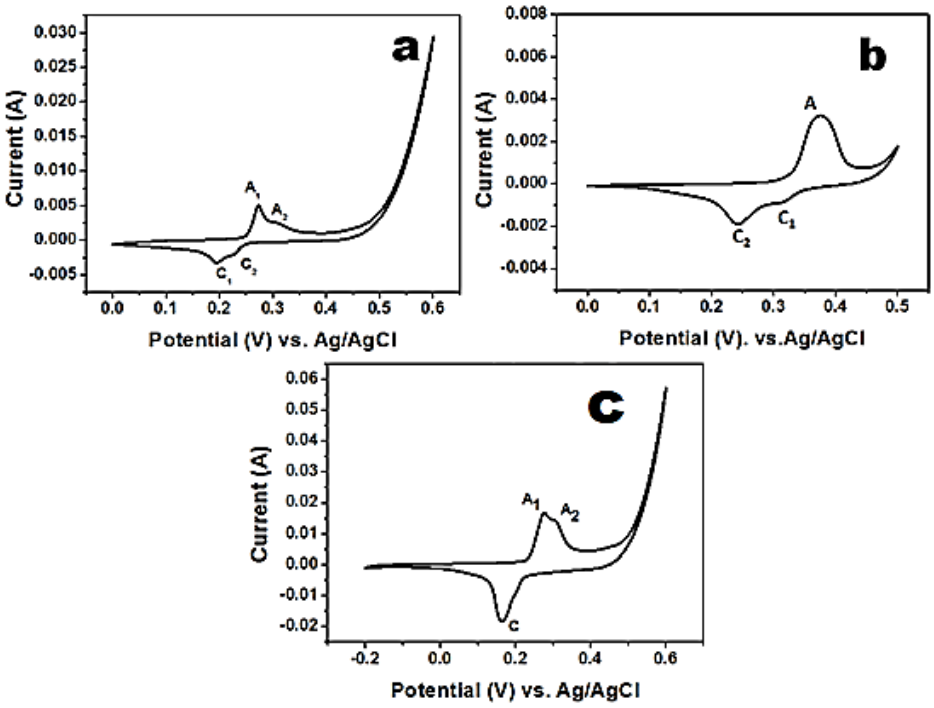

Figure 4. Cyclic Voltammograms at 2 mVs^{-1}; (a) CuO, (b) NiO, (c) NiO+CuO. A's and C's indicate oxidation and reduction events.

The C_S (Fg^{-1}) of the samples was estimated from the cathode or anodic part of the CV data using $Cs = \frac{1}{mv(E2-E1)}\left(\int_{E1}^{E2} i(E)dE\right)$, where E_1 and E_2 are the cut-off potentials in the CV curves and *i(E)* is the current at each potential, $E_2 - E_1$ is the potential window, *m* is the mass of the active material, and *v* is the scan rate. The CV measurements have been performed at various scan rates to evaluate the rate dependent pseudo capacitive performance of the samples and shown in Fig. 5. The CV profiles show oxidation (anodic) and reduction (cathode) events at all scan rate, which are characteristics of pseudocapacitors. The anodic peak in the CV profile shifted towards positive potentials with increase in the scan rate and the cathodic peak to the negative potential on account of the polarization in the electrode material. The asymmetric and scan rate dependent shape of the CV profiles show that the origin of the capacitance is by fast and reversible Faradic reaction. Slower scan rates enable higher diffusion of hydroxyl ions into the nanowire electrodes thereby accessing a major fraction of the active site in the material and show high C_S.

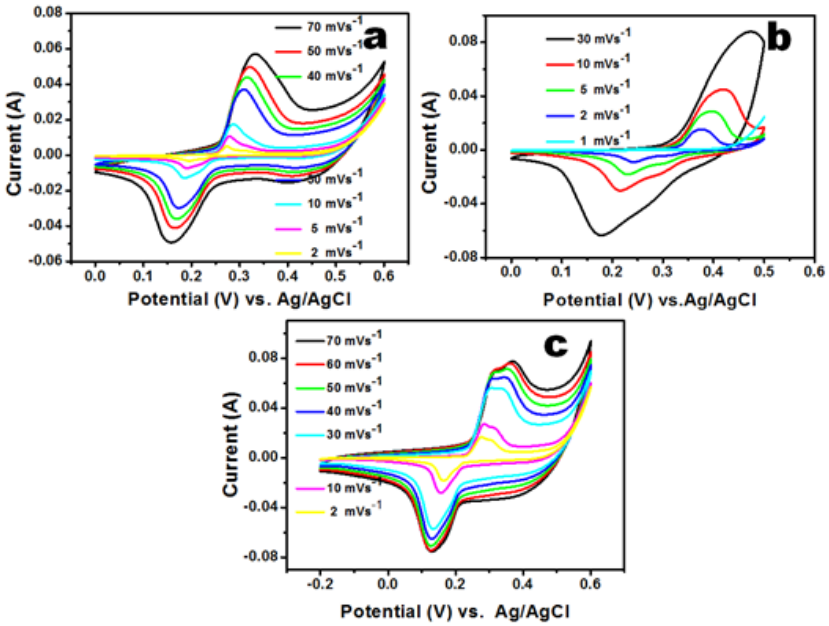

Figure 5. Cyclic Voltammograms of samples at various scan rate (a) CuO, (b) NiO, (c) NiO+CuO.

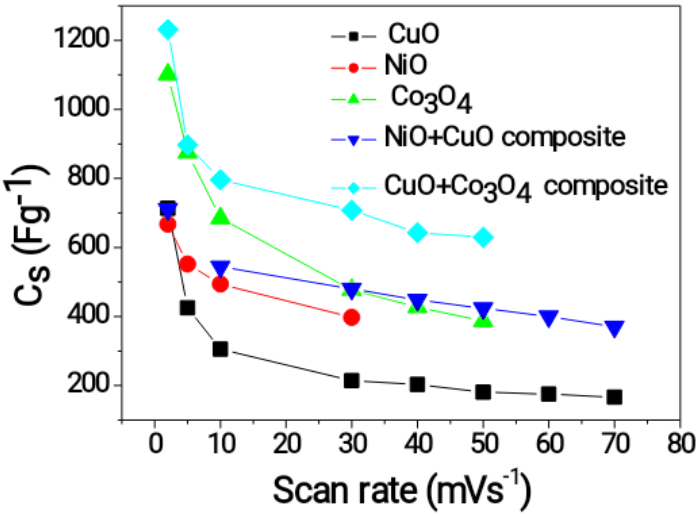

Figure 6. Variation of specific capacitance as a function of scan rate.
Data from Ref. [22] is also added for comparison.

The super capacitive performance of the ceramic oxide nanowire electrodes was evaluated from the galvanostatic CDC curves. Fig. 7(a-c) show the first three charge discharge curves of the samples at a galvanostatic current density 1 Ag^{-1} in 6M KOH. The maximum attainable potential is ~0.4 V in the KOH. For a given material system maximum attainable potential window depends on the dissociation energy of the electrolyte. Organic electrolyte and ionic electrolyte would provide wide potential window up to about ~3.5 V. The discharge curve is observed to be a combination of three processes, viz. (i) a fast initial potential drop followed by (ii) a slow potential decay, and (iii) a faster voltage drop corresponding to EDLC. The first two sections are assigned to reduction of samples as observed

from the CVs. The clear non-linear shape of the discharge curves (Fig. 7) reveal that the major contribution of C_S of the samples from Faradic reactions.

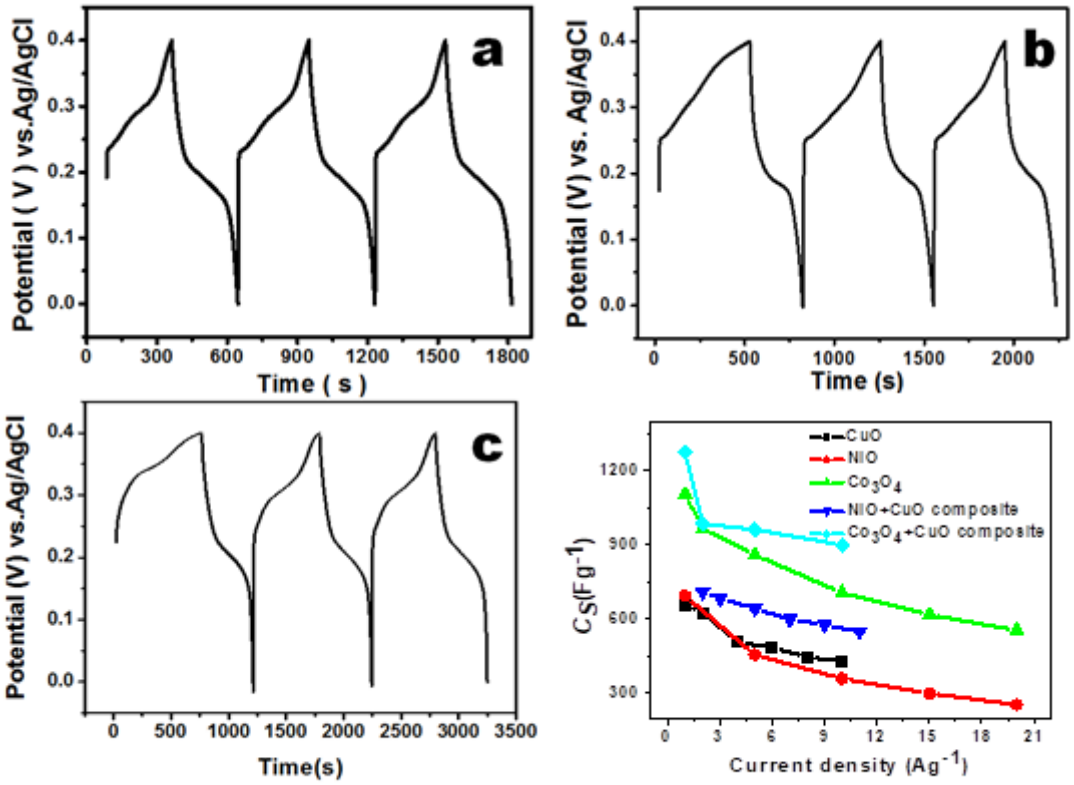

Figure 7. First three charge discharge curves; (a) CuO, (b) NiO, (c) NiO+CuO

The C_S was calculated from the discharge curve using $A = \frac{It}{m\Delta V}$, where I, t, m and ΔV are applied current, discharge time, active mass, and potential window respectively. The C_S Calculated from the discharge curve at a current density 1 Ag^{-1} for all samples is given in Table 2.

Table 2 Summary of internal resistance and C_S calculated from charge /discharge curves.

Sample	V_{IR} (mV)	I_D (mA)	Internal resistance (Ω)	C_S (Fg^{-1})
CuO	7	5	1.4	657
NiO	3	2.2	1.4	694
NiO+CuO	6	5	1.2	716

An electrode material with high life cycle stability is practically preferred for long term use in electrochemical supercapacitors. Therefore, the cyclic stability of the samples has been tested for 2000 cycles at a current density 5 Ag^{-1}. Effects of the high crystallinity of the present electrospun samples are more evident in the cycling stability of the samples in this study. Fig. 8 summarizes the stability of electrochemical cycling of the samples and their Coulombic efficiency.

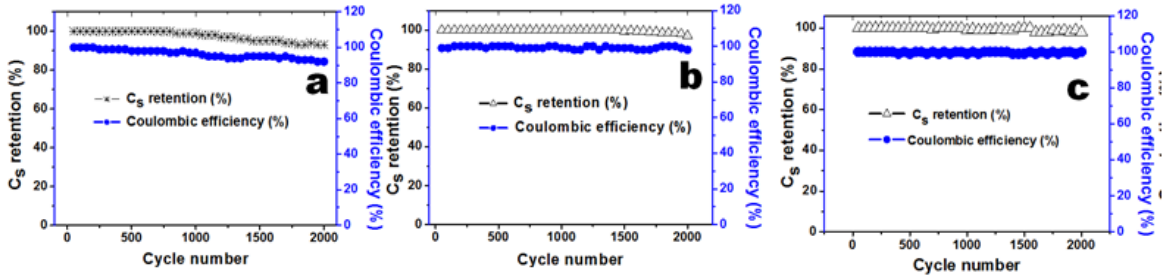

Figure 8. Dependence of the discharge specific capacitance and the Coulombic efficiency as a function of charge discharge cycle; (a) CuO, (b) NiO, (c) Co_3O_4, (d) NiO+CuO, (e) Co_3O_4+CuO.

Fig. 8(a) shows the stability of electrochemical cycling of the CuO nanowires. The electrode showed good cycling behaviour with ~99% C_S retention in 6M KOH at the end of 1000 cycles. However, a more pronounced loss in C_S was observed in the 1001 – 2000 range of cycles. A capacity fading of ~8% was observed in this range for the 6M KOH electrolytes. The electrode was physically stable; the active material stuck well with nickel foam substrate even at the end of 2000 cycles. Nevertheless, capacity fading in the present CuO nanowires is lower than that is reported for most CuO nanostructures. To be specific, compared to the ~18% capacity fading in just 500 cycles in the electrode reported the highest C_S until this work, i.e., in the CuO nanosheets synthesized using the template growth method, the capacity fading of ~10% in the present work with superior C_S for 2000 cycles is certainly advantageous. Fig. 8(b) shows the stability of electrochemical cycling of the NiO nanowires.

The electrode showed good cycling behaviour with ~100 % retention in C_S at the end of 1000 cycles thereby sharply contrasting the advantage of the present nanowires compared to previous electrospun nanowires obtained using organic solvents that marked >13% capacitance loss at similar conditions. However, a capacity loss of 6% was recorded for the present NiO wires for 2000 cycles when cycled at a rate of 5 Ag^{-1} which could be attributed to the partial irreversibility of the current material system as observed in the CV curves. Nevertheless, compared to the literature values (Table 2.4), a loss of 6% in 2000 cycles is a superior performance. The electrode was also physically stable; no peeling-off of the electrode material from nickel foam. Initial Coulombic efficiency of the NiO electrode was ~98%, which was reduced to ~94 % at the end of 2000 cycles. Fig. 8(c) shows the electrochemical stability and Coulombic efficiency of the NiO+CuO composite nanowire at a current density 5 Ag^{-1}. Apart from their single components, the capacitance of the electrode was 678 Fg^{-1} for about first 100 cycles and thereafter it reached 682 Fg^{-1} and remained same until 2000 cycles. Coulombic efficiency remained ~ 99 till the end of 2000 cycles. Fig. 5.12(e) shows the electrochemical stability and Coulombic efficiency of Co_3O_4+CuO composite nanowire electrode. The capacitance of the electrode remained same after 120 cycles until 2000 cycles; Coulombic efficiency remained ~ 100 %. The observed small increase in *Cs* value of both NiO+CuO samples during the first 100-150 CDC is usually due to initial surface activation as the electrolyte gradually penetrates into the composite structure.

4. Conclusions

In conclusion, the CuO and NiO showed extremely low diameters ~ 30 – 60 nm; however, the composite wires had a diameter ~100 nm. Improved electrical conductivity of the aqueous polymeric solution is likely the reason for the lower fiber diameters. The wires have desirable pore diameter and BET surface area for efficient electrochemical reaction. The crystal structures of the materials were studied by x-ray and electron diffraction as well as high resolution lattice images. The CuO crystallized in the space group C12/c1, #15, with lattice parameters a = 4.598 Å, b = 3.46 Å, c= 5.135 Å and β = 99.30o; the NiO crystallized in the space group, with lattice parameters a = 4.18 Å. The

composite fibers showed no shifting of lattice parameters or additional peaks. Therefore, the present method is a method for producing nanocomposites of different materials in the form of nanowires.

Electrochemical performance of CuO, NiO, and its composites NiO+CuO have been evaluated in three electrode configuration using cyclic voltammetry, and galvanostatic charge discharge cycling, Cyclic voltammetry revealed that capacitance originated from fast and reversible redox reaction and found that the samples achieved C_S nearly 30% its theoretical capacitance at low scan rate 2 mVs^{-1}; C_S are as following CuO ~627 Fg^{-1}, NiO ~671 Fg^{-1}, and NiO+CuO ~710 Fg^{-1}. All the electrodes maintained high cycling stability.

Acknowledgements
This work was supported by the Ministry of Education grant via the FRGS FRGS/1/2019/STG07/UMP/01/1.

References

[1] Elim H I, Reddy M V and Jose R 2019 A Frontier 2D Nanobattery: "Improving Challenges (Hotumese) and Development" *Sci. Nat.* **2** 114–21

[2] Reddy M V, Subba Rao G V and Chowdari B V R 2013 Metal Oxides and Oxysalts as Anode Materials for Li Ion Batteries *Chem. Rev.* **113** 5364–457

[3] Lin Z, Taberna P-L and Simon P 2017 Electrochemical double layer capacitors: What is next beyond the corner? *Curr. Opin. Electrochem.* **6** 115–9

[4] Lin Z, Goikolea E, Balducci A, Naoi K, Taberna P L, Salanne M, Yushin G and Simon P 2018 Materials for supercapacitors: When Li-ion battery power is not enough *Mater. Today* **21** 419–36

[5] Pal B, Yang S, Ramesh S, Thangadurai V and Jose R 2019 Electrolyte selection for supercapacitive devices: a critical review *Nanoscale Adv.* **1** 3807–35

[6] Pal B, Yasin A, Kunwar R, Yang S, Yusoff M M and Jose R 2019 Polymer versus Cation of Gel Polymer Electrolytes in the Charge Storage of Asymmetric Supercapacitors *Ind. Eng. Chem. Res.* **58** 654–64

[7] Ramakrishna S, Jose R, Archana P S, Nair A S, Balamurugan R, Venugopal J and Teo W E 2010 Science and engineering of electrospun nanofibers for advances in clean energy, water filtration, and regenerative medicine *J. Mater. Sci.* **45** 6283–312

[8] Vidyadharan B, Aziz R A, Misnon I I, Anil Kumar G M, Ismail J, Yusoff M M and Jose R 2014 High energy and power density asymmetric supercapacitors using electrospun cobalt oxide nanowire anode *J. Power Sources* **270** 526–35

[9] Ramaseshan R, Sundarrajan S, Jose R and Ramakrishna S 2007 Nanostructured ceramics by electrospinning *J. Appl. Phys.* **102** 111101

[10] Aghasiloo P, Yousefzadeh M, Latifi M and Jose R 2019 Highly porous TiO_2 nanofibers by humid-electrospinning with enhanced photocatalytic properties *J. Alloys Compd.* **790** 257–65

[11] Esfahani H, Jose R and Ramakrishna S 2017 Electrospun Ceramic Nanofiber Mats Today: Synthesis, Properties, and Applications *Materials* **10** 1238

[12] Aziz R A and Jose R 2017 Charge storage capability of tunnel MnO_2 and alkaline layered Na-MnO2 as anode material for aqueous asymmetry supercapacitor *J. Electroanal. Chem.* **799** 538–46

[13] Aziz R A, Muzakir S K, Misnon I I, Ismail J and Jose R 2016 Hierarchical Mo_9Se_{11} nanoneedles on nanosheet with enhanced electrochemical properties as a battery-type electrode for asymmetric supercapacitors *J. Alloys Compd.* **673** 390–8

[14] Mahmud M A, Elumalai N K, Pal B, Jose R, Upama M B, Wang D, Gonçales V R, Xu C, Haque F and Uddin A 2018 Electrospun 3D composite nano-flowers for high performance triple-cation perovskite solar cells *Electrochimica Acta* **289** 459–73

[15] Pal B, Bakr Z H, Krishnan S G, Yusoff M Mohd and Jose R 2018 Large scale synthesis of 3D nanoflowers of SnO_2/TiO_2 composite via electrospinning with synergistic properties *Mater. Lett.* **225** 117–21

[16] Bakr Z H, Wali Q, Ismail J, Elumalai N K, Uddin A and Jose R 2018 Data of chemical analysis and electrical properties of SnO_2-TiO_2 composite nanofibers *Data Brief* **18** 860–3

[17] Bakr Z H, Wali Q, Ismail J, Elumalai N K, Uddin A and Jose R 2018 Synergistic combination of electronic and electrical properties of SnO_2 and TiO_2 in a single SnO_2-TiO_2 composite nanofiber for dye-sensitized solar cells *Electrochimica Acta* **263** 524–32

[18] Ling J, Pal B, Chong K, Schmidt-Mende L, Bisquert J and Jose R 2019 Photocurrents in crystal-amorphous hybrid stannous oxide/alumina binary nanofibers *J. Am. Ceram. Soc.* **102** 6337–48

[19] Bakr Z H, Wali Q, Yang S, Yousefsadeh M, Padmasree K P, Ismail J, Ab Rahim M H, Yusoff M M and Jose R 2019 Characteristics of ZnO–SnO_2 Composite Nanofibers as a Photoanode in Dye-Sensitized Solar Cells *Ind. Eng. Chem. Res.* **58** 643–53

[20] Harilal M, Krishnan S G, Vijayan B L, Venkatashamy Reddy M, Adams S, Barron A R, Yusoff M M and Jose R 2017 Continuous nanobelts of nickel oxide–cobalt oxide hybrid with improved capacitive charge storage properties *Mater. Des.* **122** 376–84

[21] Harilal M, Krishnan S G, Yar A, Misnon I I, Reddy M V, Yusoff M M, Ojur Dennis J and Jose R 2017 Pseudocapacitive Charge Storage in Single-Step-Synthesized CoO–MnO_2–$MnCo_2O_4$ Hybrid Nanowires in Aqueous Alkaline Electrolytes *J. Phys. Chem. C* **121** 21171–83

[22] Harilal M, Vidyadharan B, Misnon I I, Anilkumar G M, Lowe A, Ismail J, Yusoff M M and Jose R 2017 One-Dimensional Assembly of Conductive and Capacitive Metal Oxide Electrodes for High-Performance Asymmetric Supercapacitors *ACS Appl. Mater. Interfaces* **9** 10730–42

[23] Mariappan C R, Gajraj V, Gade S, Kumar A, Dsoke S, Indris S, Ehrenberg H, Prakash G V and Jose R 2019 Synthesis and electrochemical properties of rGO/polypyrrole/ferrites nanocomposites obtained via a hydrothermal route for hybrid aqueous supercapacitors *J. Electroanal. Chem.* **845** 72–83

[24] Pal B, Vijayan B L, Krishnan S G, Harilal M, Basirun W J, Lowe A, Yusoff M M and Jose R 2018 Hydrothermal syntheses of tungsten doped TiO_2 and TiO_2/WO_3 composite using metal oxide precursors for charge storage applications *J. Alloys Compd.* **740** 703–10

[25] Vijayan B L, Krishnan S G, Zain N K M, Harilal M, Yar A, Misnon I I, Dennis J O, Yusoff M M and Jose R 2017 Large scale synthesis of binary composite nanowires in the Mn_2O_3-SnO_2 system with improved charge storage capabilities *Chem. Eng. J.* **327** 962–72

[26] Vidhyadharan B, Misnon I I, Aziz R A, Padmasree K P, Yusoff M M and Jose R 2014 Superior supercapacitive performance in electrospun copper oxide nanowire electrodes *J. Mater. Chem. A* **2** 6578–88

[27] Vidyadharan B, Misnon I I, Ismail J, Yusoff M M and Jose R 2015 High performance asymmetric supercapacitors using electrospun copper oxide nanowires anode *J. Alloys Compd.* **633** 22–30

[28] Vidhyadharan B, Zain N K M, Misnon I I, Aziz R A, Ismail J, Yusoff M M and Jose R 2014 High performance supercapacitor electrodes from electrospun nickel oxide nanowires *J. Alloys Compd.* **610** 143–50